Proceedings of the Canadian Society for Mechanical Engineering International Congress
32nd Annual Conference of the Computational Fluid Dynamics Society of Canada
Canadian Society of Rheology Symposium
CSME/CFDSC/CSR 2025
May 25–28, 2025, Montréal, Québec, Canada

Paper Number

Preliminary Radiator Sizing for a Polymer Electrolyte Membrane Fuel Cell Electric Aircraft

Adam Sherwood[1*], Jeremy Laliberté[1],

[1]Department of Mechanical and Aerospace Engineering, Carleton University, Ottawa, Canada
[*]AdamSherwood@cmail.carleton.ca

January 31, 2025

***Abstract*—**Fuel cell systems are becoming increasingly desirable for propulsion of sustainable, low emission aircraft. In this study, a fuel cell system consisting of a fuel cell stack, hydrogen storage, and a cowled radiator was sized to evaluate the performance impact of the radiator on a Diamond DA20 trainer aircraft. The fuel cell stack sizing is done by determining the total number of cells required to meet the power requirement, and the operating voltage is optimized for the lowest system mass. The drag from the radiator and its inlet cowl is determined through approximating their coefficients of drag, and the extra power required at the motor to overcome the drag is included in the sizing of the fuel cell. With a single pilot on board, the range of the aircraft had to be reduced from the target 973 km, to 690 km to meet the 254 kg mass requirement for the system. The hydrogen storage tank, fuel cell stack, and radiator represented 57.0%, 26.5%, and 8.8% of the system weight respectively. The hydrogen fuel and coolant represented the remaining 4.6% and 3.1%, respectively. The power required to overcome the drag from the radiator and cowl consumed 2.5% of the total power produced by the fuel cell during cruise. The findings indicate that the performance impact of the thermal management system should not be neglected in the preliminary performance assessment of fuel cell systems for aircraft propulsion.

***Keywords*—Radiator, fuel cell system, aircraft propulsion**

I. Introduction

Driven by Canadian and international initiatives to reduce greenhouse gas emissions and develop sustainable transportation fuels, hydrogen is increasingly being seen as a potential pathway for low emission aircraft propulsion [1], [2]. Fuel cells operating on low-carbon hydrogen have been identified as a possible technology for converting hydrogen into useful electrical power. One of the key technology areas for fuel cell systems is the thermal management system [3]. In contrast to to the high temperatures seen in combustion systems, a low-temperature polymer electrolyte membrane (PEM) fuel cell operates in the 50°C to 90°C range. Fuel cells also operate at thermal efficiencies around 50%, meaning that for every kilowatt of electrical power produced, one kilowatt of heat is produced.

Liquid cooling is the most practical approach for the larger (>5 kW) fuel cell systems seen in transportation [3], [4]. With liquid cooling, a heat exchanger is necessary to reject the added heat in the coolant. The heat exchanger typically takes the form of a radiator. The added weight and drag from the radiator corresponds to reduced cargo capacity and increased thrust requirements, respectively. Therefore, evaluating the weight and drag of the radiator can improve the initial feasibility assessment of a fuel cell system for an aircraft.

Zhang and Kandlikar [5] present a parameterized physical model of a radiator for a fuel cell aircraft, creating sizing correlations for the radiator. Additionally, Schröder et. al [6], and Massaro et. al [7], present overall fuel cell system sizing optimizations, both using the effectiveness-NTU method for the radiator sizing. In this work, an iterative sizing methodology for a fuel cell stack, hydrogen storage tank, and cowled radiator is presented. Sec. II presents the methods used in determining the aircraft's flight profile, the model for the fuel cell, sizing of the radiator, and the overall system sizing. Sec. III displays the results for the given aircraft and discusses the implications of these results.

II. Methodology

A. Aircraft Flight Profile

The aircraft selected for analysis is the Diamond DA20-C1, which is a single-engine trainer aircraft. The shaft power, altitude, and velocity for each phase of flight was determined from the manufacturer's Pilot Operating Handbook (POH).

The peak shaft power requirement, cruise altitude, and cruise velocity are 93 kW, 8000 ft, and 60 m/s, respectively. The selected design range of the hypothetical fuel cell powered aircraft was set to 973 km to match the maximum range of the original internal combustion engine powered aircraft [8]. However, the range was reduced in Sec. III to decrease the mass of the overall system. The model assumes the system is under steady-state operating conditions at each phase of flight, therefore the dynamics of the system are neglected. For phases with changing conditions (i.e. climb, takeoff, etc.), the phase is split into sub-phases. The flight profile for a maximum range mission is shown in Fig. 1, with the sub-phases shown as the intermediate steps in the figure. The number of sub-phases in each phase was selected to be sufficiently high that the results were independent of the number of sub-phases. Where the range is changed, the time in cruise is modified, with no changes to the other phases.

The fuel cell power shown in Fig. 1a) represents the required net output power from the fuel cell, considering the stack-to-shaft losses in the system. The stack-to-shaft losses consider the losses from the power electronics, electric motor, and electrical distribution, and has been approximated at 90%. Shaft power is used for propeller aircraft, as opposed to thrust, which is used for jet aircraft. The same propeller losses are assumed for the unmodified and hypothetical fuel cell electric aircraft.

B. Fuel Cell Model

The fuel cell is modelled as a generic PEM fuel cell, following the procedure and parameters outlined by Geyer and Ahluwalia [9]. The overall fuel cell voltage is calculated from four inputs: the reference voltage, activation losses, Ohmic losses, and concentration losses. The reference voltage E_0 is the theoretical voltage of a PEM fuel cell under a given temperature and reactant concentration, and is approximated via [9]:

$$E_0 = 1.05 + 0.055 \log_{10}(P_{c,O_2,in}) \tag{1}$$

where $P_{c,O_2,in}$ is the partial pressure of oxygen in the air inlet in bar.

The activation losses represent the voltage required to start the reaction and are modelled via the Tafel equation [10]:

$$v_{act} = C_1 \log_{10}(j/j_0) \tag{2}$$

where j is the current density (in A/cm^2), C_1 is an empirical coefficient equal to 0.055, and j_0 is the exchange current density, approximated as 10^{-3} A/cm^2 [9].

The Ohmic losses represent the ionic and electronic resistance of the membrane and electrodes via:

$$v_\Omega = R_\Omega A_m j \tag{3}$$

where the resistance R_Ω is calculated through [9]:

$$R_\Omega = \frac{1.0604 - 2.493 \cdot T_{cell} 10^{-3}}{A_m} \tag{4}$$

where T_{cell} and A_m are the temperature of the cell (in K), and the active area of the membrane (in cm^2), respectively.

Lastly, the concentration losses occur when the consumption rate of the reactants approaches the supply rate, and this is modelled though:

$$v_{conc} = 0.1 \log_{10}\left(1 - \frac{j}{j_{lim}}\right) \tag{5}$$

where j_{lim} is the maximum current density (in A/cm^2), defined as:

$$j_{lim} = 1.4 + 3.924\left(\frac{P_{c,O_2,in}}{P_{c,in}} - 0.21\right) + 0.2(P_{c,in} - 3) \tag{6}$$

where $P_{c,in}$ is the total air-side inlet pressure in bar.

The overall cell voltage is determined through:

$$v_{cell} = E_0 - (v_{act} + v_\Omega + v_{conc}) \tag{7}$$

and the resulting polarization curve for 90°C, and an absolute inlet pressure of air at 250 kPa is shown in Fig. 2. The polarization curve describes a fuel cell's electrical behaviour, relating the current density to the operating voltage. The current density is the current draw per unit of cell active area. The voltage directly affects the fuel efficiency, since a higher voltage results in a higher power for the same amount of hydrogen consumed.

The fuel cell stack is sized by determining the number of cells required to meet the peak power output. The active area of a cell has been defined at 240 cm^2 to match [11]. Excluding the power required to overcome the drag of the radiator, which is discussed in Sec. II-C, the power required to operate the balance-of-plant components has been chosen as 10% of the desired net power output. This parasitic power must be used

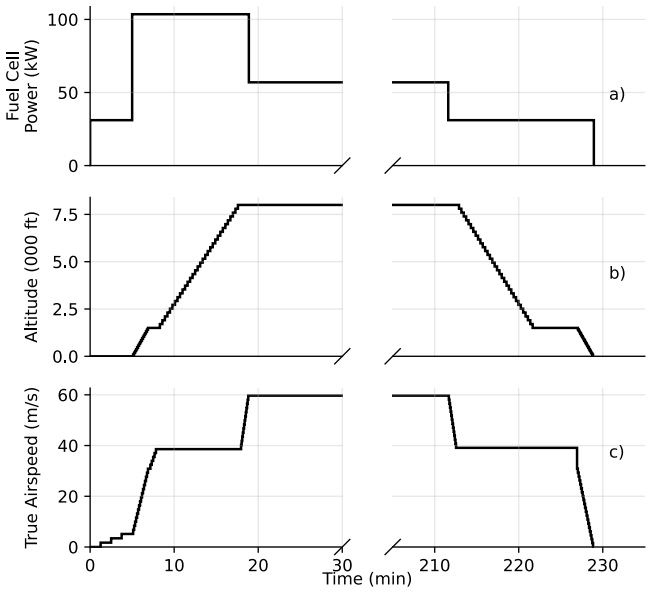

Figure. 1: Target flight profile with a 973 km range showing a) fuel cell output power, b) flight altitude, and c) true airspeed.

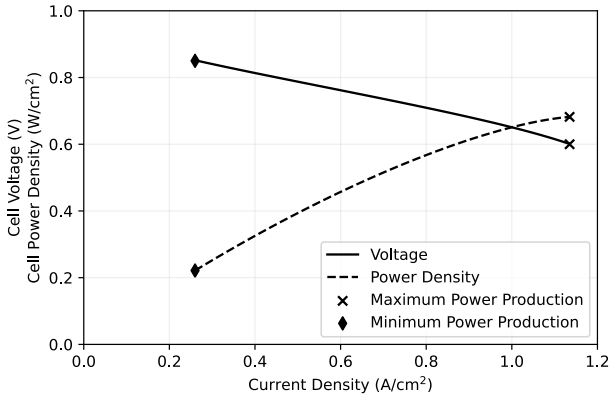

Figure. 2: Fuel cell polarization curve.

to compress the inlet air, and other non-propulsive loads. The number of cells is determined via:

$$n_{cells} = \text{ceil}\left(\frac{P_{net,max} + P_{aux,max} + P_{rad,max}}{P_{cell,max}}\right) \quad (8)$$

where $P_{net,max}$ is the maximum net power, seen as 103 kW from Fig. 1, $P_{rad,max}$ is the peak power draw to overcome the radiator drag, $P_{aux,max}$ is the power required for the other balance-of-plant components, and $P_{cell,max}$ is the power produced by a single cell at the design cell-level voltage, determined from the polarization curve.

The design cell-level voltage is a parameter that is optimized in Sec. III. This parameter defines at what voltage a single cell in the stack should operate when the peak power is requested. If the design cell-level voltage is set to 0.6 V, then the cells will be operating at the cell's maximum power production point shown in Fig. 2. This case represents the smallest stack, however it is the least fuel efficient since the voltage is lowest. Instead, the design cell-level voltage can be increased to decrease fuel consumption, at the cost of stack weight. The maximum and minimum power production points represent the lowest and highest operational voltages from the stack, respectively. A range of 0.6 V to 0.85 V is often used to prevent the increased degradation that occurs outside this range. The mass of the fuel cell stack is determined using a power density of 2.0 kW/kg [11] and the power at the stack's maximum power production point.

The heat generated at each phase of flight can also be determined through the polarization curve and the power requirement, through:

$$\dot{Q}_{gen} = (1.225 - v_{cell}) \cdot i \cdot n_{cells} \quad (9)$$

where i is the current produced from a cell. The total amount of hydrogen required to complete the flight is found through:

$$m_{H_2} = \frac{M_{H_2}}{2F \cdot \eta_{vent}} \int i(t)dt \quad (10)$$

where $i(t)$ is the current produced by the fuel cell at time t, M_{H_2} is the molar mass of hydrogen gas, F is the Faraday

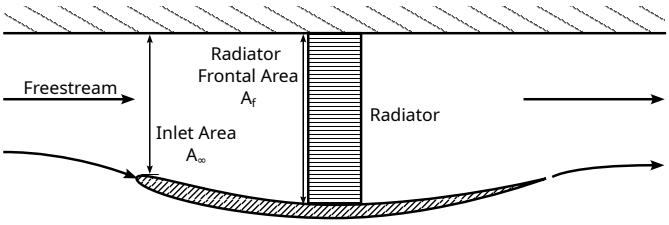

Figure. 3: Cowled radiator design, adapted from [13].

Constant (96 485 A.s/mol), and η_{vent} is 98%, accounting for the hydrogen that is lost from venting to purge nitrogen from the line.

The mass of the storage tank is then calculated using a 7.5% storage efficiency for a 350 bar Type 4 tank [12]. The storage efficiency is defined as:

$$\eta_{storage} = \frac{m_{H2}}{m_{tank} + m_{H2}} \quad (11)$$

C. Radiator Design

A cowled radiator design is used as it reduces drag and increases cooling performance relative to a radiator without a cowl [13]. The cowl decelerates the flow before it reaches the radiator, then accelerates it after. The design is shown in Fig. 3. The radiator frontal area to inlet flow area ratio A_f/A_∞ is used to describe the change in flow parameters from ambient conditions into the radiator inlet conditions. The optimal value of this parameter is found in Sec. III as it affects the cooling performance and drag of both the radiator and the cowl.

To estimate the performance, the aircraft-specific methodology described by Drela [13] is adapted. The hydraulic radius of the air channels of the radiator is defined though the length of the channel l, open area ratio σ, radiator frontal area A_f and the overall heat transfer area A_h through:

$$r_h = \frac{l\sigma A_f}{A_h} \quad (12)$$

The hydraulic radius and channel length were approximated at 0.228 mm, and 25.3 cm, respectively, based on plate-fin aircraft radiators from [14]. The open area ratio is treated as a parameter that will be evaluated between 0.65 and 0.85, as per the limits seen in the historical aircraft radiators shown in [14].

To simplify the mathematics and provide information on the boundary layer, a passage parameter ξ following [13] is defined that includes the kinematic viscosity μ, the density ρ_1, and the flow velocity into the radiator channel v_1 via:

$$\xi^2 = \frac{l\sigma\mu}{r_h Pr \rho_1 v_1 r_h} \quad (13)$$

A low ($<< 1$) passage parameter ξ represents a case where the majority of the radiator's outlet flow from the air channel is unaffected by the boundary layer. A high (> 1) passage parameter represents the situation when the boundary layer affects most of the radiator's air channel.

The governing equations were derived from [13] and [15] using the average Reynolds scaled Colburn Modulus J to get the overall heat transfer coefficient K_h:

$$K_h = JRe^{\frac{1}{2}} \tag{14}$$

$$J = StPr^{2/3} \tag{15}$$

where J is the Colburn Modulus, Re, St, and Pr are the Reynolds number, Stanton number and Prandtl number, respectively. The Stanton number relates the overall heat transferred to a fluid to its thermal capacity, and can be written as:

$$St = \frac{\dot{Q}/A_h}{C_p(T_r - T_1)\rho_1 v_1/\sigma} \tag{16}$$

where $\dot{Q}$ is the heat transfer rate, T_r and T_1 are the average coolant temperature and air inlet temperature, respectively, and C_p is the coolant specific heat capacity, assumed as constant. Equation (16) is combined with (12), (13), and (14) to form an equation for the heat transfer rate:

$$\dot{Q} = \xi K_h C_p (T_r - T_1) Pr^{-1/6} \rho_1 v_1 A_f \tag{17}$$

The frontal area of the radiator is then determined through

$$A_f = \frac{\dot{Q} Pr^{1/6}}{\xi K_h C_p (T_r - T_1)\rho_1 v_1} \tag{18}$$

With the frontal area, the mass of the radiator is determined using an area density factor. The factor was determined from the data sheet of a radiator designed for a transport truck, since a truck radiator is an example of a modern radiator designed for transportation. The area density factor was calculated at 65.9 kg/m^2 [16], which also agrees with the ranges shown for historic aircraft radiators in [14].

The drag caused by the radiator and cowl is overcome by increasing the power from the electric motor, resulting in a higher required fuel cell power. The drag of the radiator is estimated by modelling the radiator as a perforated plate. The methodology presented in [17] was used to obtain the relationship between the core's open area ratio and its coefficient of drag relative to the frontal area, through:

$$C_D = \frac{4}{3}\frac{(1-u^*)(2+u^*)}{2-u^*} \tag{19}$$

$$C_D = u^{*2}\left(\frac{1}{\sigma^2} - 1\right) - \frac{4}{3}\frac{(1-u^*)^3}{(2-u^*)^2} \tag{20}$$

Where u^* is determined iteratively such that the two equations are equal. The results of which are shown in Fig. 4.

The cowl drag is determined assuming an airfoil of constant coefficient of drag of 0.05, based on the frontal area. More accurate approximations can be determined through more complex means such as the relationship with the airfoil's angle of attack (α) through C_d/α curves, however this is outside the scope of the preliminary evaluation presented in this paper.

The required fuel cell power to offset the drag from the cowled radiator is found via

$$P_{drag} = \frac{\sum_i v_i \cdot D_i}{\eta_{prop} \cdot \eta_{stack-to-shaft}} \tag{21}$$

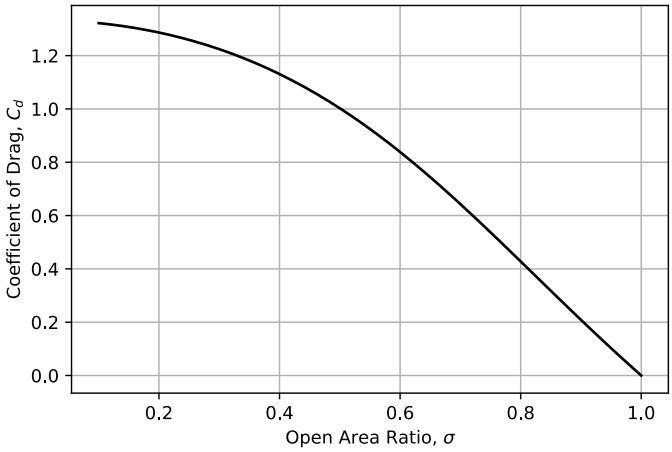

Figure. 4: Radiator core coefficient of drag, as a perforated plate, adapted from [17].

where v_i and D_i are the flow velocity and drag, respectively, for component i (cowl, radiator), η_{prop} is the propulsive efficiency at 85%, and $\eta_{stack-to-shaft}$ is the stack-to-shaft efficiency. The flow velocity for the cowl is the free-stream velocity, whereas the radiator's velocity is determined through the isentropic flow relations for the area change.

The mass of the coolant is determined using the peak coolant flow rate based on historical data on automotive truck cooling systems. Using the coolant capacity data presented in [18], and peak flow rate data presented in [19], the circulation time for the coolant system is 6 seconds. For the aircraft's coolant capacity, peak heat rejection is determined with a desired coolant temperature difference of 10°C. The coolant is a 50/50 split of ethylene glycol and water, as is common for aircraft.

D. System Sizing

The general system sizing methodology is shown in Fig. 5 and all steps were implemented in Python. Since the fuel cell stack and radiator sizes depend on each other, an iterative sizing approach was employed. Starting with the net power requirement from the stack for propulsive power, an initial guess of the radiator drag offset power is made to inform the sizing of the stack. After the stack is sized, the heat generated from the stack is used to size the radiator and calculate the drag offset power. If the new radiator drag power is different from the value used to size the fuel cell stack, the stack is resized, and the process is repeated. Once the drag offset power has converged, the sizing stage is complete. The radiator uses the ambient conditions at sea level with the aircraft at cruise velocity for the worst-case drag from the radiator at cruise.

After the sizing, a point analysis is run to evaluate the performance of the system at each of the phases of flight. The point analysis assumes that the system dynamics occur on a timescale much smaller than the overall system, and therefore each phase of flight is considered to be at steady state, with no changes in speed, altitude, power, or aircraft mass.

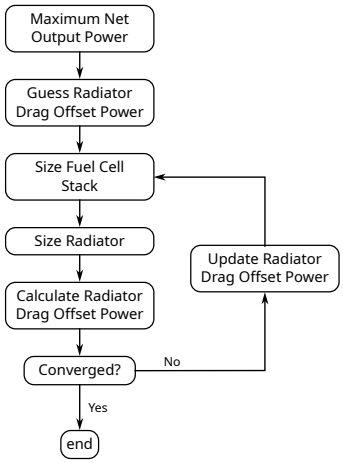

Figure. 5: Iterative system sizing flowchart

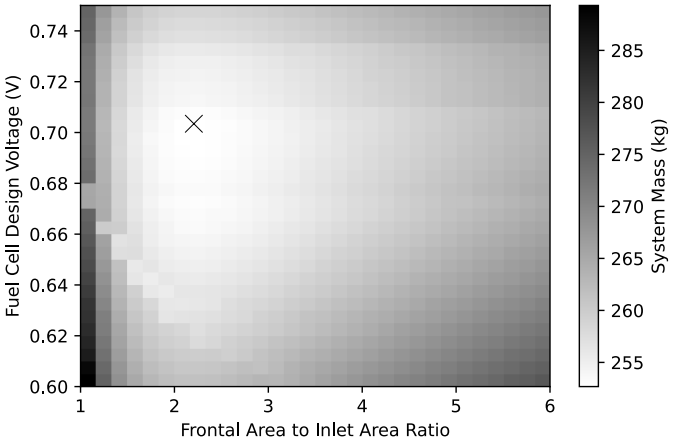

Figure. 6: Fuel cell design voltage and frontal area to inlet area optimization for system mass, with the lowest mass marked.

For performance evaluation, a system efficiency parameter is defined as:

$$\eta_{sys} = \frac{P_{net}}{\dot{m}_{H_2} LHV_{H2}} \tag{22}$$

where P_{net} is the power provided by the fuel cell for propulsion, $\dot{m}_{H_2}$ is the hydrogen consumption rate, and LHV_{H2} is the lower heating value of hydrogen (33.33 kWh/kg).

III. Results and Discussion

The useful payload of the unmodified aircraft is 265 kg [8]. This payload can be increased by 85.2 kg by replacing the piston engine (115 kg [20]) with an equivalent power electric motor (22.3 kg [21]) and motor controller (7.5 kg [22]) resulting in 350 kg for the fuel cell propulsion system and the useful payload. Considering a single 96 kg pilot [23], the mass of the fuel cell system would need to be less than 254 kg. Evaluating the system at different ranges indicates that the aircraft's maximum range is not achievable with the current fuel cell system, since the optimal mass was calculated to be 324 kg. However, the mass requirement is met at a range of 690 km, a 29% reduction in range.

It was also determined that maximizing the open area ratio σ resulted in the lowest mass, therefore it was set to a constant 0.85. The fuel cell's design voltage at peak power was plotted with the frontal area to inlet area ratio A_f/A_∞ to see their effects on the system mass. Fig. 6 shows this result, with the optimal mass occurring at a design cell voltage of 0.703 V, and an area ratio of 2.21. In Fig. 6, the system mass is most sensitive to the area ratio, with the mass increasing significantly close to a value of 1. The frontal area of the radiator was calculated as 0.337 m^2, meaning that the inlet area is 0.152 m^2, leading to 40.3 N of drag during cruise. Therefore, the radiator assembly results in an increase in the aircraft's total drag by 6.0% in cruise. The drag from the radiator represented 92.1% of the radiator assembly drag, with the remaining 7.9% coming from the cowl.

The masses of each component are shown in Tab. I. The heaviest component is the storage tank, followed by the fuel cell, then the radiator. It is important to note that the presented mass does not include the other auxiliary components for the fuel cell system, such as the humidifier, piping, and instrumentation. When the additional components are included, their mass can be offset by further reductions to the range, further reducing the storage tank mass.

TABLE. I: System mass breakdown for 690 km range mission.

Component	Mass (kg)	% of System Mass
Storage Tank	144	57.0%
Fuel Cell Stack	67.0	26.5%
Radiator	22.2	8.8%
Hydrogen	11.7	4.6%
Coolant	7.8	3.1%

The peak heat generation from the fuel cell stack was 85.7 kW during the takeoff and climb. The total power and heat generation from the fuel cell stack with 842 cells is shown in Fig. 7a). The minimum voltage seen during the flight is 0.703 V, which occurs at the end of the transition between climb and cruise. This operating point is important because both the power and velocity are at a maximum, meaning that the drag power is also at a maximum, which can be seen in Fig. 7b). The voltage reaches the minimum power production point during the taxi, descent, approach, and landing phases. In these phases, the average requested net power of 31.1 kW is less than the minimum power production point of 42.4 kW, therefore the cells operate at the minimum power production point, wasting the 11.3 kW of power. From Fig. 1, the total power produced by the fuel cell during cruise is 56.9 kW, and the drag power during cruise is 1.4 kW, therefore the drag power consumes 2.5% of the fuel cell power during cruise. The effect of changing altitudes on the drag can be seen during the climb and descent phases in Fig. 7b), where the speed is constant but the altitude changes.

In Fig. 7c), the system efficiency is between 50.3% and 63.1%, with higher efficiencies corresponding to lower power draws because of the higher fuel cell voltage. At the lowest efficiency of 50.3%, both the velocity and fuel cell power are

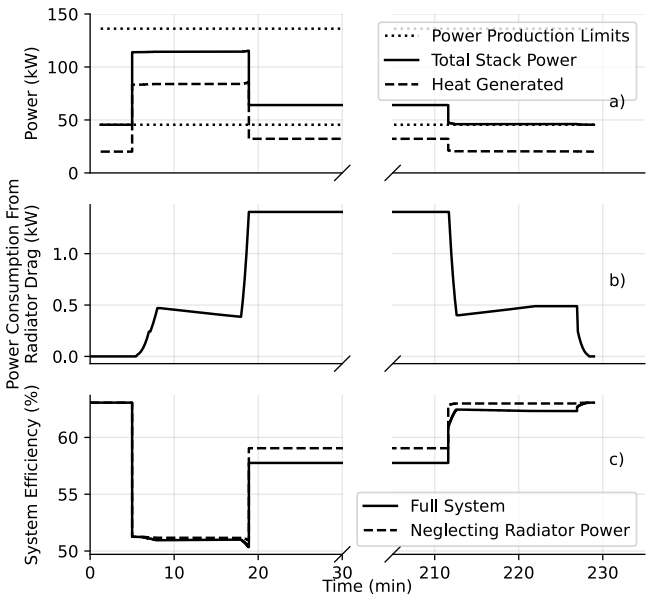

Figure. 7: Results for a) the total power production from the stack, compared with the power production limits from the stack, b) the power consumed to offset the radiator drag, and c) the overall system efficiency for the 690 km flight.

at a maximum, since the aircraft is at the end of the transition from climb to cruise. If the drag power from the radiator is neglected, as shown as the dashed line in Fig. 7c), then the cruise efficiency would increase from 57.8% to 59.1%.

Larger aircraft are expected to see a more significant performance impact from the radiator system because of the higher heat generation from the stack, and the drag force scaling with the square of the velocity, however this is the focus of future work. The system's volume, and the other balance-of-plant components, will also be included in future work.

IV. Conclusions

This paper presents the sizing of the fuel cell stack, hydrogen storage, and cowled radiator for a small fuel cell electric aircraft. The mass and drag of these components were determined to quantify their effects on the aircraft takeoff weight and performance. The range of the aircraft had to be reduced from 973 km to 690 km for a single pilot crew to meet the mass requirement. The storage tank represented 57.0% of the total mass. As expected, the second-heaviest component was the fuel cell stack, representing 26.5%, and the radiator represented 8.8%, plus 3.1% for the coolant. The last 4.6% of the system mass was taken up by the hydrogen fuel. The impact of the drag from the radiator was less than that of the mass but still significant, with the radiator and cowl drag consuming 2.5% of the total power produced by the fuel cell during cruise. The inclusion of the radiator had a non-negligible effect on the overall system efficiency.

V. Acknowledgements

This research was supported by the National Research Council of Canada (NRC) and Defence Research and Development Canada (DRDC) through the Greening Government Fund project: Canadian Low Emissions Aircraft Platforms. The authors would like to acknowledge Paul Paterson from Redrock Power Systems, and Natesa MacRae from the NRC for their technical expertise on hydrogen and fuel cell systems.

References

[1] Natural Resources Canada, "The hydrogen strategy." https://natural-resources.canada.ca/climate-change/canadas-green-future/the-hydrogen-strategy/23080, 2024. Accessed: 23-12-2024.

[2] International Civil Aviation Organization (ICAO), "Climate change." https://www.icao.int/environmental-protection/pages/climate-change.aspx, 2024. Accessed: 21-01-2025.

[3] M. Ramezanizadeh, M. A. Nazari, M. H. Ahmadi, and L. Chen, "A review on the approaches applied for cooling fuel cells," *International Journal of Heat and Mass Transfer*, vol. 139, pp. 517–525, 2019.

[4] G. Zhang and S. G. Kandlikar, "A critical review of cooling techniques in proton exchange membrane fuel cell stacks," *international journal of hydrogen energy*, vol. 37, no. 3, pp. 2412–2429, 2012.

[5] R. d. S. Collares, *A thermal management system parametric model for fuel cell powered aircraft conceptual design*. PhD thesis, Universidade de São Paulo, 2024.

[6] M. Schröder, F. Becker, and C. Gentner, "Optimal design of proton exchange membrane fuel cell systems for regional aircraft," *Energy Conversion and Management*, vol. 308, p. 118338, 2024.

[7] M. C. Massaro, S. Pramotton, P. Marocco, A. H. A. Monteverde, and M. Santarelli, "Optimal design of a hydrogen-powered fuel cell system for aircraft applications," *Energy Conversion and Management*, vol. 306, p. 118266, 2024.

[8] Diamond Aircraft, "Da20 series - space, speed and style - diamond aircraft indsutries," 2024. https://www.diamondaircraft.com/en/flight-school-solution/aircraft/da20/overview/.

[9] H. Geyer and R. Ahluwalia, "Gctool for fuel cell systems design and analysis: User documentation," *Argonne National Laboratory*, 1998.

[10] F. Barbir, *PEM fuel cells: theory and practice*. Academic press, 2012.

[11] T. Yoshida and K. Kojima, "Toyota mirai fuel cell vehicle and progress toward a future hydrogen society," *The Electrochemical Society Interface*, vol. 24, no. 2, p. 45, 2015.

[12] Luxfer Gas Cylinders, "Alternative Fuel: G-Stor Go H2 Carbon Composite Type 4 Cylinders," 2024. https://www.luxfercylinders.com/product/g-stor-go-h2-type-4-carbon-composite-cylinders/.

[13] M. Drela, "Aerodynamics of heat exchangers for high-altitude aircraft," *Journal of aircraft*, vol. 33, no. 1, pp. 176–184, 1996.

[14] S. Parsons and D. Harper, "Radiators for aircraft engines," *Journal of the Washington Academy of Sciences*, vol. 11, no. 17, pp. 409–416, 1921.

[15] W. S. Janna and R. P. Chhabra, *Design of fluid thermal systems*, vol. 4, ch. 10.3, pp. 522–537. Cengage Learning Stamford Place, 2015.

[16] Dolphin Manufacturing LLC, "Freightliner radiator, year 2008-2014 — dolphin catalogue," 2024. Accessed: 30-12-2024.

[17] K. Steiros and M. Hultmark, "Drag on flat plates of arbitrary porosity," *Journal of Fluid Mechanics*, vol. 853, p. R3, 2018.

[18] B. Flannery, O. Finckh, H. Berresheim, and R. F. Monaghan, "Hybrid stirling engine-adsorption chiller for truck auxiliary power unit applications," *international journal of refrigeration*, vol. 76, pp. 356–366, 2017.

[19] E. Nordlander, "Modelling and validation of a truck cooling system," 2008.

[20] European Union Aviation Safety Agency, *Continental IO-240 series engines*, 2020. https://www.easa.europa.eu/en/document-library/type-certificates/engine-cs-e/easaime169-continental-io-240-series-engines.

[21] EMRAX, "268 (210kw — 500nm) - emrax," 2024. https://emrax.com/e-motors/emrax-268/.

[22] emDrive Mobility, "emDrive H300 datasheet V1.7," 2024. https://www.emdrive-mobility.com/portfolio/emdrive-h300/.

[23] Transport Canada - Civil Aviation Reference Centre, "Advisory circular (ac) no. 700-022 - air operator weight and balance control procedures," 2019. Accessed: 23-05-2023.